

PAPER

mr-EBL: ultra-high sensitivity negative-tone electron beam resist for highly selective silicon etching and large-scale direct patterning of permanent structures

To cite this article: Adriaan J Taal *et al* 2021 *Nanotechnology* **32** 245302

View the [article online](#) for updates and enhancements.



The Electrochemical Society
Advancing solid state & electrochemical science & technology

240th ECS Meeting ORLANDO, FL

Orange County Convention Center Oct 10-14, 2021



Abstract submission due: April 9

SUBMIT NOW

mr-EBL: ultra-high sensitivity negative-tone electron beam resist for highly selective silicon etching and large-scale direct patterning of permanent structures

Adriaan J Taal^{*} , Jake Rabinowitz  and Kenneth L Shepard 

Electrical Engineering, Columbia University, New York, United States of America

E-mail: at3111@columbia.edu, jake.rabinowitz@columbia.edu and shepard@ee.columbia.edu

Received 8 March 2020, revised 25 February 2021

Accepted for publication 11 March 2021

Published 25 March 2021



Abstract

Electron beam lithography (EBL) is the state-of-the-art technique for rapid prototyping of nanometer-scale devices. Even so, processing speeds remain limited for the highest resolution patterning. Here, we establish Mr-EBL as the highest throughput negative tone electron-beam-sensitive resist. The $10 \mu\text{C cm}^{-2}$ dose requirement enables fabricating a 100 mm^2 photonic diffraction grating in a ten minute EBL process. Optimized processing conditions achieve a critical resolution of 75 nm with $3\times$ faster write speeds than SU-8 and 1–2 orders of magnitude faster write speeds than maN-2400 and hydrogen silsesquioxane. Notably, these conditions significantly differ from the manufacturers' recommendations for the recently commercialized Mr-EBL resist. We demonstrate Mr-EBL to be a robust negative etch mask by etching silicon trenches with aspect ratios of 10 and near-vertical sidewalls. Furthermore, our optimized processing conditions are suitable to direct patterning on integrated circuits or delicate nanofabrication stacks, in contrast to other negative tone EBL resists. In conclusion, Mr-EBL is a highly attractive EBL resist for rapid prototyping in nanophotonics, MEMS, and fluidics.

Keywords: electron beam lithography, nanofabrication, reactive ion etching, Raman spectroscopy, diffraction grating, negative tone resist, high sensitivity

(Some figures may appear in colour only in the online journal)

1. Introduction

Electron beam lithography (EBL) and direct-write electron beam assembly are established techniques for rapid and nanometer-scale device prototyping with applications in photonics [1], electronics [2], 2D materials [3], and catalysts [4]. EBL prototyping is particularly useful in nanoscale photonics, where new paradigms of light manipulation can be realized by creating solid-state structures with dimensions similar to optical wavelengths (i.e. $0.1\text{--}2 \mu\text{m}$).

EBL resists come in positive and negative tones. Positive resists offer high resolution and easy removal, making for excellent wet etch and lift-off masks in metal deposition. In

contrast, negative tone resists [5] cross-link into chemically inert molecules, making for excellent masks in substrate dry etching [6]. Additionally, processed negative resist becomes a permanent structure, making it well suited to the direct fabrication of nanoimprint lithography templates [7], or permanent optical [8, 9], microfluidic [10], or microelectromechanical [11] structures.

Contrast and sensitivity are key factors when choosing an EBL resist. Contrast determines the minimum possible feature size and sensitivity determines the speed of processing. The two factors correlate strongly for negative EBL resists (figure 1(a)) despite not being fundamentally related. Among highly sensitive negative resists, SU-8 is the current gold standard [12], despite low contrast limiting its resolution to

^{*} Author to whom any correspondence should be addressed.

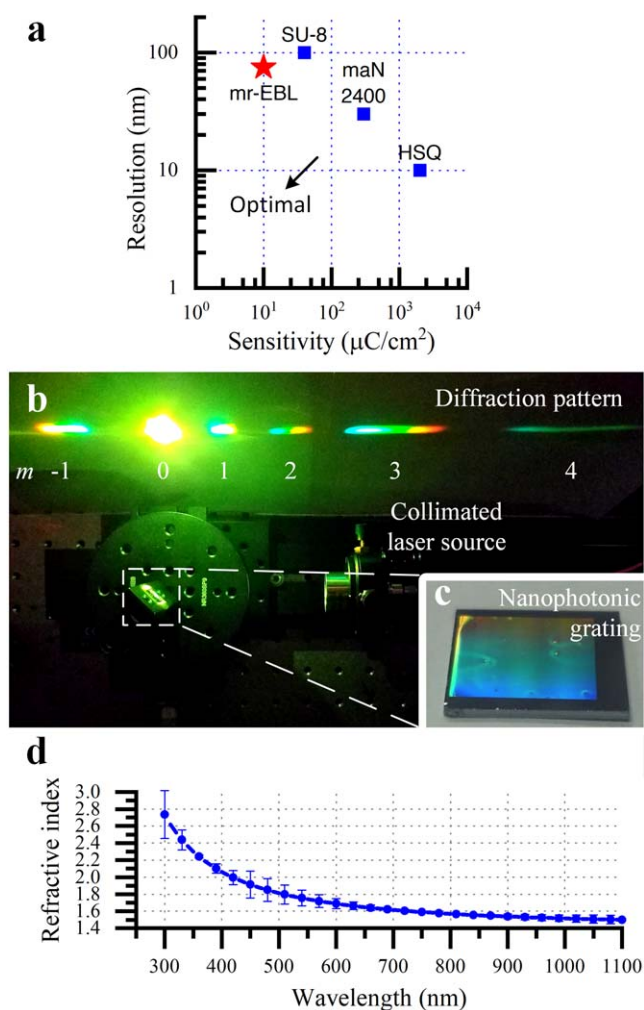


Figure 1. (a) Sensitivity versus resolution for commonly used negative tone electron beam lithography resists. (b) Reflective diffraction grating fabricated with Mr-EBL resist. The diffraction orders (m) are annotated. (c) The large-area (100 mm^2) binary phase grating is fabricated on silicon in under ten minutes. (d) Refractive index versus wavelength in the VIS-NIR range for cross-linked Mr-EBL resist.

~100 nm. Widespread use of SU-8 is also limited by poor adhesion to common substrate materials.

Other negative EBL resists, such as hydrogen silsesquioxane (HSQ) and maN-2400, achieve excellent contrast and resolution. However, these resists require large exposure doses due to their low sensitivities: $\sim 300\text{ }\mu\text{C cm}^{-2}$ for maN-2400 [13] and $\sim 2000\text{ }\mu\text{C cm}^{-2}$ for HSQ [14] when processing with a 100 kV electron beam. These high dose requirements limit iteration speed and throughput during device prototyping. Similarly to SU-8, maN-2400 adheres poorly to silicon and glass, requiring extra adhesion promoting steps for successful use [15]. For HSQ, a low refractive index ($n = 1.4$) [16] limits photonics applications where light manipulation is enabled by the large refractive index difference between the device and its surrounding medium. Finally, HSQ and maN-2400 are only soluble in alkaline developers, which can strip off metal films and make these resists incompatible with integrated circuits or other supporting electronics.

In this paper, we demonstrate rapid and large-scale EBL prototyping using the Mr-EBL 6000.3 (MicroResist Technology) negative tone resist. We fabricate a 100 mm^2 diffraction grating in a direct patterning approach that requires less than 10 min. This capability establishes Mr-EBL as an attractive resist for ultra-high-throughput EBL with significantly accelerated nanofabrication speed when compared to alternate resists. We show Mr-EBL to deliver state-of-the-art sensitivity, excellent adhesion, high refractive index, and organic solvent-based development. We present optimized processing parameters for maximizing resolution and contrast. We conclude with pre- and post-processed chemical analyses to identify the monomer cross-linking mechanism induced during electron beam exposure.

2. Experimental methods

2.1. Application

We demonstrate the applicability of Mr-EBL to nanoscale photonics by fabricating a large-area reflective diffraction grating on silicon with a single-step direct patterning process. We verify the grating by projecting a supercontinuum laser source (EXU-6PP, NKT photonics) through a collimator and onto the grating surface. The spectral bandwidth of the laser is set to 100 nm around a center wavelength of 550 nm through a tunable line filter (SuperK Varia, NKT Photonics).

2.2. Resist processing

Substrates are cleaned with acetone and isopropyl alcohol before spin coating Mr-EBL at 6000 RPM for a nominal thickness of 250 nm. To achieve a thickness of 50 nm, we dilute one part Mr-EBL 6000.3 to three parts anisole. The resist is soft baked for 3 min at $110\text{ }^\circ\text{C}$ to evaporate the carrier solvent (Anisole). The resist is exposed with an Elionix ELS-G100 EBL system. The beam diameter is confined to 1.8 nm by using a 100 pA beam current at 100 kV. Proximity error correction software (Beamer) locally alters electron doses to sharpen sparse patterns and prevent overexposure of dense patterns. Following exposure, the resist is fully cross-linked through a soft post exposure bake (PEB) for 1 min at $80\text{ }^\circ\text{C}$. Crosslinked resist is developed for 5 min at room temperature in propylene glycol methyl ether acetate (PGMEA, SU-8 developer, Microchem) or propylene carbonate (Alfa Aesar) and then rinsed thoroughly with isopropyl alcohol. The patterned resist is made permanent by hard baking for 120 min at $120\text{ }^\circ\text{C}$, with 15 min ramp-up and ramp-down times.

2.3. Characterization

2.3.1. Resolution. Resolution is determined by writing $15 \times 15\text{ }\mu\text{m}$ patterns that vary line widths and spacings in 25 nm increments. Minimum widths consider the smallest fully resolved and completely intact structures. Line edge roughness conveys the reliability of resolving these minimum widths. Resolution and line edge roughness values for the

250 nm thick resist are determined through inspection on a Zeiss Sigma VP scanning electron microscope at 20 kV with 3 mm working distance. Linewidths correspond to the mean widths of the imaged lines and line-edge roughnesses are determined by the standard deviations of the linewidths over the $15 \times 15 \mu\text{m}$ pattern, as calculated by image processing algorithms in MATLAB.

The 50 nm thick resist was topographically imaged with a Bruker Dimension Icon atomic force microscope (AFM).

2.3.2. Contrast. For negative tone EBL resists, contrast refers to the width of the transition regime between the highest exposure dose without cross-linking and the lowest exposure dose to induce cross-linking. We calculate contrast (γ) of the exposed $15 \times 15 \mu\text{m}$ regions as [17]:

$$\gamma = \frac{1}{\log_{10} \frac{D_{90}}{D_{10}}}, \quad (1)$$

where D_{90} corresponds to the clearing exposure dose for 90% resist height retention after development (near-complete cross-linking) and D_{10} corresponds to the onset exposure dose for 10% resist height retention after development (minimal cross-linking). These doses are determined by AFM-based topographic profiles of post-processed resist.

2.3.3. Raman spectroscopy. Elastic resonances of atomic bonds are measured with a Renishaw InVia micro-Raman using an excitation laser at 532 nm. Chemical compositions are deduced from scattering peak locations and intensities in the 0–3000 cm^{-1} range.

2.3.4. Refractive index. Refractive indices are determined with a Woollam V-VASE ellipsometer. We model the interaction between light and dielectrics with a Lorentz oscillator function by fitting the real part of the refractive index to polarization and intensity data collected from reflecting light off of the resist. A two-term Sellmeier dispersion model, fit to the ellipsometer data using the least squares approach, smooths the refractive index (n) as a function of wavelength (λ) [18]:

$$n^2(\lambda) = A + \frac{B_1 \lambda^2}{\lambda^2 - C_1} + \frac{B_2 \lambda^2}{\lambda^2 - C_2}, \quad (2)$$

where A is a constant approximation for the short-wavelength contribution, B_n are scaling constants and C_n are spectral shifting constants.

2.4. Dry etching

Patterned resist is processed with an inductively coupled plasma reactive ion etch (ICP-RIE). We investigate the etch selectivity for two plasma chemistries: sulfur hexafluoride (SF_6) [19] and hydrogen bromide (HBr) [20] in an Oxford PlasmaLab 100. The SF_6 etching is conducted at 20 W forward and 2000 W coil power, with $\text{SF}_6:\text{C}_4\text{F}_8:\text{O}_2:\text{Ar}$ flowrates of 30:30:5:30 SCCM at 8 mTorr pressure. The HBr etching is conducted at 10 W forward and 1900 W coil power, with

20 SCCM flowrate at 20 mTorr pressure. After etching, any residual resist is stripped by inductively coupled oxygen plasma etching. Etched resist thickness and silicon trench depth are measured using a Bruker Dektak-XT stylus profilometer. The corresponding selectivities are determined by comparing the resist and silicon etch rates.

3. Results

3.1. Rapid prototyping

Typical nanofabrication efforts incorporate complex and serial steps of film deposition, lithography, etching, and resist stripping. These processes greatly limit the throughput of device prototyping, particularly in light conditioning applications underlying integrated photodetection [21], laser-to-waveguide coupling [22], and photonic crystals [23]. We substitute the multi-step fabrication processes for rapid direct structure writing, demonstrating Mr-EBL to significantly improve the speed, cost, and compatibility of rapid device prototyping in nanophotonic and other applications.

We show Mr-EBL to be favorable to alternative negative tone EBL resists when comparing the trade-offs between resolution and throughput (figure 1(a)). Mr-EBL offers $3\times$ faster processing speeds and 25% better resolution when compared to SU-8. When compared to HSQ and maN, Mr-EBL offers $30\text{--}200\times$ faster processing speeds with only a $4\text{--}8\times$ loss in resolution.

We demonstrate a rapidly prototyped light conditioning structure by directly writing a diffraction grating with Mr-EBL (figure 1(b)). The resist's high sensitivity allows for writing of a large 100 mm^2 binary phase grating onto a silicon substrate in under 10 min.

The nanostructured Mr-EBL resist induces self-interference of an incident wave front to reflect light with a wavelength-dependent angle. When a broad spectrum incident light source is obliquely directed ($\vartheta_i = 45^\circ$) at the diffraction grating (figure 1(c)), the spectral-angular conditioning reveals itself as color bands (figure 1(b)).

We verify the intended diffraction behavior by observing one negative diffraction order ($m = -1$) and four positive diffraction orders ($m = 1, 2, 3, 4$) (figure 1(b)). At the $m = 0$ diffraction order, the absence of light conditioning is revealed by the circular non-diffracted pattern.

The observed diffraction patterns confirm that the Mr-EBL resist was fabricated as intended. From left to right ($m = -1$ to 4), the green bands ($\lambda = 550 \text{ nm}$) of the diffraction orders (θ_m) are positioned at 90° , 45° , 23° , 6° , -11° and -28° relative to the grating normal (figure 1(b)). These angles coincide with the expected diffraction pattern, as predicted by the grating pitch (p), incident light angle (ϑ_i), incident light wavelength (λ), and resist refractive index (n):

$$\theta_m = \text{asin}\left(\sin(\vartheta_i) - \frac{m\lambda}{np}\right). \quad (3)$$

Based on the EBL pitch of $1 \mu\text{m}$ and a measured refractive index of 1.8 (figure 1(d)), we predict diffraction order

angles of 90° , 44° , 23° , 6° , -12° and -31° , consistent with observations.

We measure the refractive index of Mr-EBL to solve equation (3) and verify the high refractive index across all wavelengths of interest to photonics applications. Refractive index values range from 1.51 to 2 in the near-infrared to the visible spectrum, reaching up to 2.7 in the near-UV range (figure 1(d)). The error bars correspond to the mean fitting error over three devices. We attribute the larger error in the 450–600 nm spectrum to larger measurement noise caused by ambient light. We note that the post-exposure refractive index is negligibly different from the pre-exposure measurement. The high refractive index is useful for photonic crystal or diffraction grating applications where an index contrast to an immersion or encapsulation medium (such as glass, aqueous solution, or oil) is required.

Resist adhesion is found to be excellent to all silicon and fused silica substrates, as assessed by applying and pulling-off polyimide tape. Similar adhesion is not achieved to noble metals, where the resist was pulled off during the tape test. To achieve proper adhesion to inert polymer substrates such as cross-linked SU-8, we treat the substrate with a brief oxygen plasma, immediately followed by spincoating hexamethyldisilazane (HMDS) until dry, before spincoating Mr-EBL.

Throughout Mr-EBL processing, we never observe peeling, resist cracking, delamination, or other indications of film stress. Patterned resist structures are chemically inert, as evidenced by being unaffected after 72 h immersions in N-methylpyrrolidone at 100°C (an aggressive resist-stripping treatment).

3.2. Resolution

The clean and large-area pattern demonstrates successful Mr-EBL writing with 150 nm minimum linewidth (figure 2(a)). At the same critical dimensions, circles and squares retain crisp edges with minimal distortion (figure 2(b)). Fabricated linewidths of 152 nm are achieved for exposure widths of 150 nm, with only 20 nm line edge roughness (figure 2(c)). Across figures 2(a)–(c), exposure doses are $14\ \mu\text{C cm}^{-2}$ and resist thickness is 250 nm. This thickness is well-suited to nanophotonics applications as it represents a quarter-wavelength optical path length difference for propagation of 600 nm light through the resist dielectric when interfaced with air.

The minimum Mr-EBL resolution is achieved by decreasing resist thickness to 50 nm while retaining the $14\ \mu\text{C cm}^{-2}$ exposure dose (figure 2(d)). The thinner resist provides more favorable aspect ratios for small features, such that 75 nm linewidths are achieved at 150 nm pitch. A single line scan from the AFM image in figure 2(d) reveals structural aspect ratios of 0.7 at the lateral resolution limit (figure 2(e)). However, the line edge roughness at this thickness (3.9 nm, averaged over two devices) precludes the resolution of smaller feature sizes.

Because the thicker resist is better suited to photonics applications, we return to 250 nm thick films to characterize the dependence of linewidth and line edge roughness on the

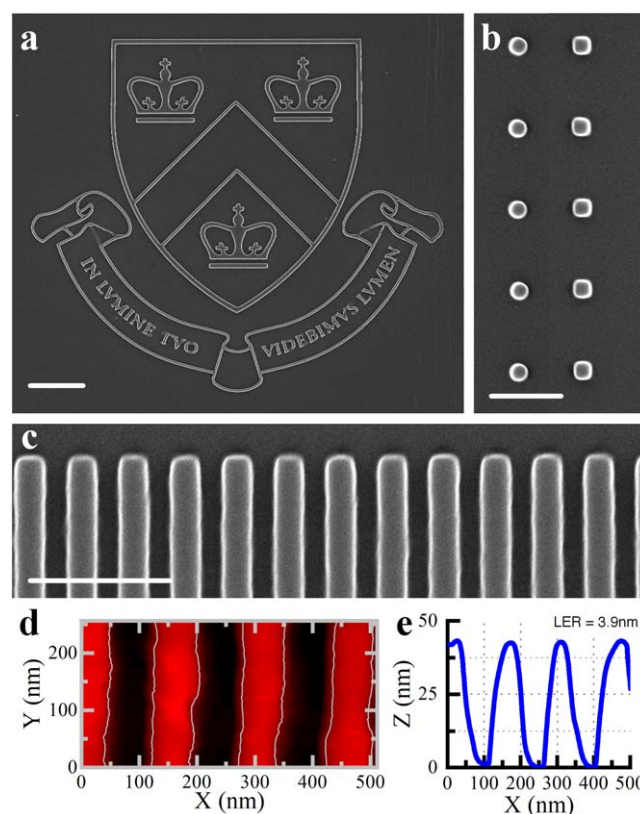


Figure 2. (a) Columbia University logo with minimum feature size of 150 nm; scalebar: $4\ \mu\text{m}$. (b) Circles and squares with feature sizes of 150 nm at a resist thickness of 250 nm; scalebar: $1\ \mu\text{m}$. (c) Lines with 150 nm width and 300 nm pitch at a resist thickness of 250 nm; scalebar: $1\ \mu\text{m}$. (d) Finest resolution lines with 75 nm width are achieved at a resist thickness of 50 nm. Contour lines depict Mr-EBL edges where resist heights reduce by half. (e) Single line scan for the area imaged in (d).

exposure dose and PEB temperature (figure 3). Intermediate dose rates ($9\text{--}14\ \mu\text{C cm}^{-2}$) and PEB temperature (80°C) achieve the best resolution of 150 nm (figure 3(a)), with a structural aspect ratio of 1.7. For less optimized processing conditions, the minimum resolutions are slightly larger (200–300 nm) and line edge roughness are mostly unchanged (20–30 nm) (figure 3(b)). Therefore, we determine the optimal processing conditions as a $14\ \mu\text{C cm}^{-2}$ dose and an 80°C PEB, for achieving a linewidth of 150 nm and a line edge roughness of 16 nm. To further accelerate prototyping speed, the same resolution is achievable with a lower dose of $10\ \mu\text{C cm}^{-2}$, at the cost of slightly increased line edge roughness.

3.3. Contrast

Contrast (γ) is an important figure of merit for resist performance. High contrast indicates greater selectivity of the developer to unexposed resist compared to exposed resist, resulting in higher aspect ratios and better resolution during EBL. We determine contrast values by measuring patterned resist step heights for varying exposure doses and developer solvents (figure 4), achieving maxima of $\gamma = 1.9$ with

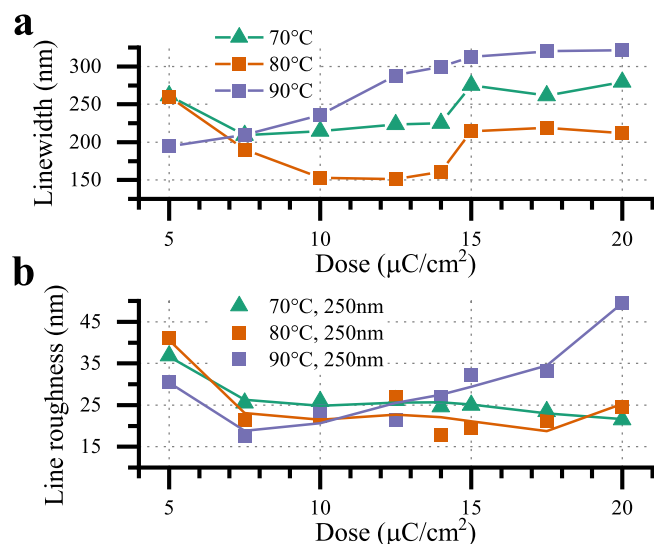


Figure 3. (a) Minimum EBL linewidth as a function of dose and post exposure bake at a resist thickness of 250 nm. (b). Line edge roughnesses for the resolutions in (a), defined as the standard deviations of the linewidths.

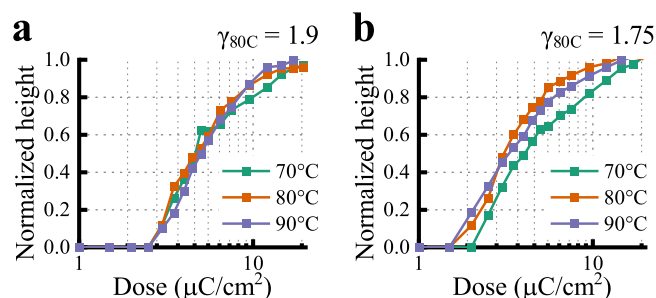


Figure 4. Resist height as a function of exposure dose and post exposure bake (PEB), for (a) propylene carbonate and (b) propylene glycol methyl ethylene acetate. For both developers, a PEB of 80 °C achieves the optimal contrast.

propylene carbonate (figure 4(a)) and $\gamma = 1.75$ with the manufacturer-recommended PGMEA (figure 4(b)). These Mr-EBL contrast values are better than those achieved in SU-8 [24, 25]. Similar to maN-2400 [5, 13], and lower than HSQ [26]. Moreover, Mr-EBL is the only resist to offer organic solvent-based development, which is more compatible with integrated circuitry and other delicate nanofabrication stacks. Similar efforts to develop HSQ with an organic solvent [27] show strongly deteriorated resolution and line edge roughness compared to alkaline solution development.

The contrast of the patterned Mr-EBL varies with PEB temperature and developer choice. The optimal contrast ($\gamma = 1.9$) is achieved with propylene carbonate for an 80 °C PEB and varies minimally across other experimental temperatures (figure 4(a)). The small clearing dose of $10 \mu\text{C cm}^{-2}$ is consistent with using this exposure dose for very high throughput EBL. The contrast decreases ($\gamma = 1.75$) and becomes more dependent on the PEB temperature for PGMEA development (figure 4(b)). The worse contrast at 70 °C ($\gamma = 1.4$) is due to reduced cross-linking reactions at the lower temperature; the worse contrast at 90 °C ($\gamma = 1.55$)

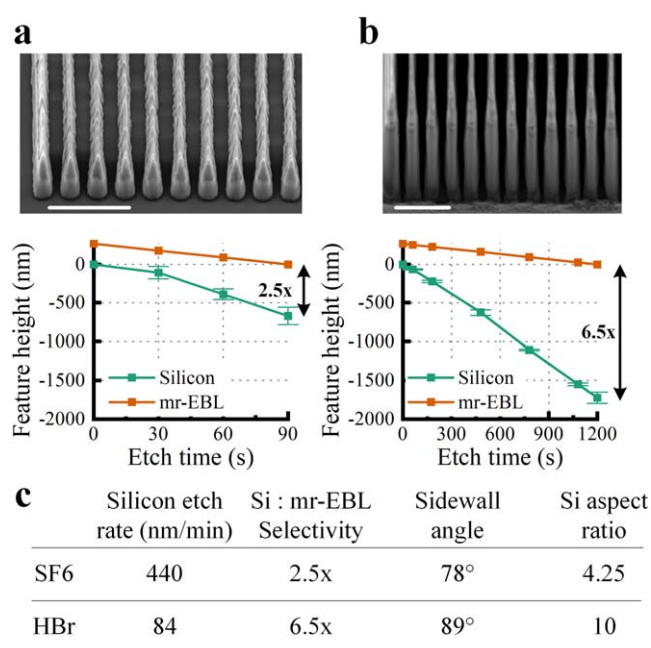


Figure 5. Etch resistance and selectivity during inductively coupled plasma reactive ion etching (ICP-RIE) of silicon using (a) SF₆ plasma and (b) HBr plasma; scalebars: 1 μm . The highly selective HBr plasma permits the fabrication of trenches deeper than 1.5 μm at a width of 150 nm. (c) Table of etch results.

indicates excessive thermally-induced cross-linking at the higher temperature, consistent with larger minimum linewidths and line edge roughnesses (figure 3). We further observe leftover resist residue after PGMEA development, which is not present when developing with propylene carbonate. To even further improve EBL throughput, at the cost of minimal resolution, we note that PGMEA reduces the clearing dose to $7.5 \mu\text{C cm}^{-2}$ at 80 °C.

3.4. Dry etch selectivity

A popular use for negative tone resists is as dry etch masks for ICP-RIE of silicon. In these applications, being chemically inert offers negative tone resists high etch selectivities versus silicon [28–31].

We demonstrate Mr-EBL as a dry etch mask by transferring EBL patterns into silicon using ICP-RIE. The etching fabricates high aspect ratio trenches with superb etch selectivities for HBr and SF₆ plasma chemistries (figure 5). We note that SEM images in figure 5 are taken at the exposure dose and dimension location in figure 2(c) after silicon etching. During etching, the process is continued until all of the resist is consumed.

Three-dimensional silicon aspect ratios of 10 (figures 5(a)) and 4 (figure 5(b)) are respectively achieved with HBr and SF₆ plasmas. HBr exhibits excellent selectivity of 6.5 \times while SF₆ is slightly worse at 2.5 \times (figure 5(c)). For SF₆, we attribute the slower initial etch rate to surface oxide presenting an etch barrier. Near-perfect sidewall angles are measured for trenches etched in HBr plasma (89°), with slightly worse performance for SF₆ plasma (78°). This discrepancy is attributed to a more isotropic etch reaction

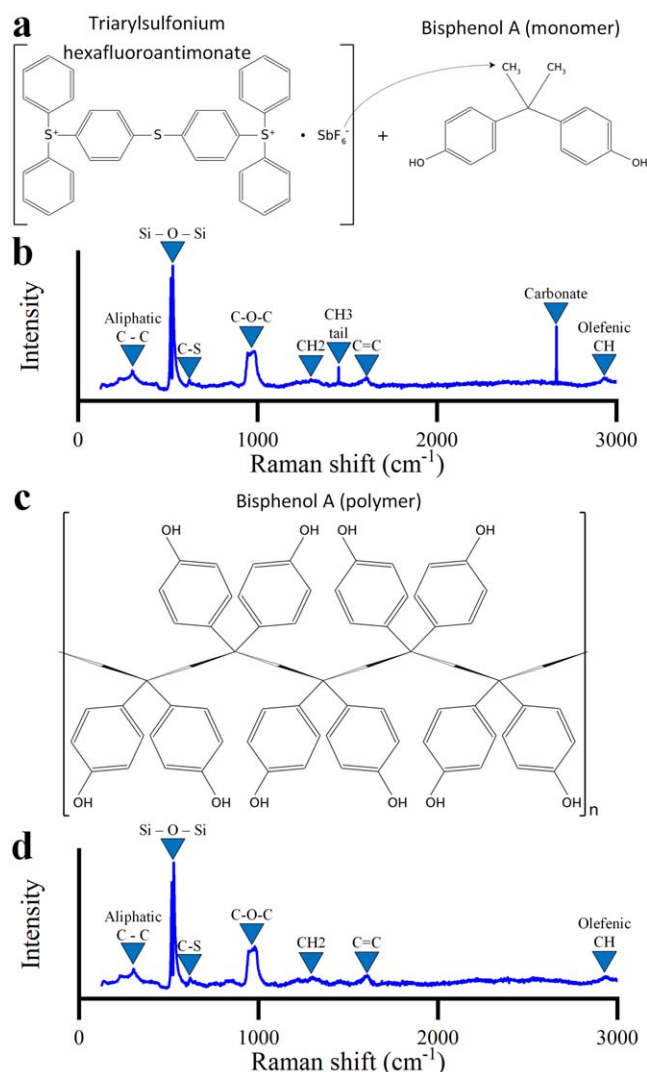


Figure 6. (a) The unexposed resist is a mixture of bisphenol-A and triarylsulfonium hexafluoroantimonate. (b) Raman spectrum of unexposed resist. (c) The resist cross-links at the methyl groups, creating a scaffold molecular structure. (d) Raman spectrum of exposed resist on silicon. The Raman spectra are corrected for the sloping baseline.

resulting in faster etching of edges when using SF₆ [32]. The etch selectivity of Mr-EBL in HBr plasma exceeds that of maN-2400, HSQ [33] and SU-8 [12].

3.5. Chemical analysis

The pre- and post-exposure chemical structure of Mr-EBL is integral to assessing its performance metrics and suitability to prospective applications. However, this information is absent from the manufacturer's datasheet.

To address this, we perform pre- and post-exposure chemical analysis and identify the cross-linking mechanism that occurs during Mr-EBL processing. Upon electron beam exposure and post-exposure baking, patterned Mr-EBL resist is made insoluble through cross-linking of bisphenol A (figure 6(a)) [34, 35]. The cross-linking reaction is catalyzed

by triarylsulfonium hexafluoroantimonate, which serves as a deep UV and electron beam sensitive photo acid generator [36–39]. The presence of these constituent molecules is confirmed in the Raman spectra measured prior to the exposure step (figure 6(b)). The pre-exposure spectrum also indicates the presence of propylene carbonate solvent, which enables uniform spin coating of the monomer-catalyst mixture. Peaks in figure 6(b) are annotated according to the relevant molecular bonds [40], for ease of correlation with the structures shown in figure 6(a).

Bisphenol A polymerization during Mr-EBL processing (figure 6(c)) is evidenced by alterations in the pre- and post-exposure chemical compositions (figures 6(b), (d)). The disappearance of the Raman peak at 1451 cm⁻¹ (figure 6(d)) corresponds to a loss of terminal methyl groups [41]. This is consistent with the cross-linking of these groups during formation of a bisphenol A scaffold network (figure 6(c)) that renders exposed resist insoluble to the developer. The removal of the peak at 2666 cm⁻¹ is attributed to evaporation of propylene carbonate solvent and corresponding loss of the carbonate bond [42]. We note that the photo acid initiator remains present after cross-linking, as indicated by the sulfur bonds around 620 cm⁻¹ [43, 44].

4. Discussion

The most widely used negative tone EBL resists are limited in their processing speed and compatibility with integrated circuits or complimentary nanofabrication protocols. This work establishes Mr-EBL 6000.3 as a negative tone EBL resist for overcoming these limitations, particularly in direct fabrication of durable structures for nanophotonics applications.

The suitability of Mr-EBL to rapid prototyping of nanophotonic devices is demonstrated through the fabrication of a large-scale optical diffraction grating in a direct write process. The 100 mm² optical grating is fabricated in under ten minutes.

Optimized Mr-EBL processing parameters are provided for achieving a lateral resolution of 150 nm with a resist thickness (250 nm) ideal for the conditioning of visible light. A minimum lateral resolution of 75 nm is achieved with thinner resist films (50 nm). For applications with larger critical dimensions (i.e. 200–300 nm), even faster processing speeds are achievable.

As a dry etch mask, we show Mr-EBL to present high etch selectivity over silicon, enabling the fabrication of deep silicon trenches with near-perfectly vertical sidewalls.

We augment the current understanding of the underlying Mr-EBL chemistry by describing the molecular cross-linking induced during electron-beam excitation and thermal catalysis.

Compared to alternative negative tone electron beam resists, we highlight three distinct advantages of Mr-EBL: (i) high sensitivity enables fast iteration of very large-scale device fabrication; (ii) organic solvent development greatly improves the resist compatibility with integrated circuits or typical nanofabrication stacks; and (iii) high refractive index

over the visible spectrum provides a suitable index contrast for light conditioning with a wide spectrum of immersion media.

With our optimized processing, Mr-EBL addresses many of the limitations of SU-8. Mr-EBL improves by half the 200 nm minimum resolution achieved for dense patterning of thin SU-8 [12, 45–47]. The lower contrast of SU-8 is due to fundamental chemical effects that causes incident electron energy to propagate further into the nearby regions and backscatter more heavily [48–50]. Several non-commercially available resists claim sensitivity comparable to Mr-EBL at 100 nm resolution, but do not show intact structures [51] or dense features [52].

It is important to note that our findings disagree with the manufacturer's datasheet on several optimized processing parameters [53]. First, we found that the recommended PEB (110 °C, 5 min) strongly limits resolution due to excessive thermally-induced cross-linking. Second, we observe increased sensitivity at our higher accelerating voltage, despite the expectation that greater electron mean free path reduces sensitivity at high voltages. We suspect our sensitivity improvement is due to exposure optimization using the Beamer software.

Finally, all the above-noted advantages of Mr-EBL are achieved without compromising contrast, resolution, or ease of use. These characteristics make Mr-EBL a promising material for rapid development of nanoscopic devices across many fields including nanophotonics, fluidics, microelectromechanical systems, and more.

Acknowledgments

We thank Gaurang Bhatt for supplying the etch recipes. This work was performed in part at the CUNY Advanced Science Research Center NanoFabrication Facility.




Data availability statement

All data that support the findings of this study are included within the article (and any supplementary files).

Funding

This work was supported in part by the Defense Advanced Research Projects Agency (DARPA) under Contract N6600117C4012 and by the National Institutes of Health under Grant U01NS090596.

ORCID iDs

Adriaan J Taal  <https://orcid.org/0000-0002-1649-2826>
 Jake Rabinowitz  <https://orcid.org/0000-0001-9671-6860>
 Kenneth L Shepard  <https://orcid.org/0000-0003-0665-6775>

References

- [1] Højlund-Nielsen E, Greibe T, Mortensen N A and Kristensen A 2014 Single-spot e-beam lithography for defining large arrays of nano-holes *Microelectron. Eng.* **121** 104–7
- [2] Bhuvana T and Kulkarni G U 2008 Highly conducting patterned Pd nanowires by direct-write electron beam lithography *ACS Nano* **2** 457–62
- [3] Zhang W, Zhang Q, Zhao M Q and Theil Kuhn L 2013 Direct writing on graphene 'paper' by manipulating electrons as 'invisible ink' *Nanotechnology* **24** 27
- [4] Zhang W, Liu Z Q and Furuya K 2008 Fabrication and characterization of cellular iron nanocrystalline film *Nanotechnology* **19** 1–6
- [5] Bilenberg B *et al* 2006 Comparison of high resolution negative electron beam resists *J. Vac. Sci. Technol. B* **24** 1776–9
- [6] Blideran M M *et al* 2009 Improving etch selectivity and stability of novolak based negative resists by fluorine plasma treatment *Microelectron. Eng.* **86** 769–72
- [7] Chou S Y 2012 Nanoimprint lithography *Nanofabrication Handbook* (Boca Raton: CRC Press) (<https://doi.org/10.1201/b11626>)
- [8] Yang C C and Chen W C 2002 The structures and properties of hydrogen silsesquioxane (hsq) films produced by thermal curing *J. Mater. Chem.* **12** 1138–41
- [9] Pang L, Nakagawa W and Fainman Y 2003 Fabrication of two-dimensional photonic crystals with controlled defects by use of multiple exposures and direct write *Appl. Opt.* **42** 5450–6
- [10] Mali P, Sarkar A and Lal R 2006 Facile fabrication of microfluidic systems using electron beam lithography *Lab Chip* **6** 310–5
- [11] Abgrall P, Conedera V, Camon H, Gue A M and Nguyen N T 2007 SU-8 as a structural material for labs-on-chips and microelectromechanical systems (review) *Electrophoresis* **28** 4539–51
- [12] Bilenberg B *et al* 2006 High resolution 100 kV electron beam lithography in SU-8 *Microelectron. Eng.* **83** 1609–12
- [13] Voigt A, Elsner H, Meyer H G and Gruetzner G 1999 Nanometer patterning using ma-N 2400 series DUV negative photoresist and electron beam lithography *Emerging Lithographic Technologies III* 3676
- [14] Lauvernier D, Vilcot J-P, François M and Decoster D 2004 Optimization of HSQ resist e-beam processing technique on GaAs material *Microelectron. Eng.* **75** 177–82
- [15] Voigt A, Ahrens G, Heinrich M, Thompson A and Gruetzner G 2014 Improved adhesion of novolac and epoxy based resists by cationic organic materials on critical substrates for high volume patterning applications *Advances in Patterning Materials and Processes XXXI* (<https://doi.org/10.1117/12.2046258>)
- [16] Choi S, Word M J, Kumar V and Adesida I 2008 Comparative study of thermally cured and electron-beam-exposed hydrogen silsesquioxane resists *J. Vac. Sci. Technol. B* **26** 1654–9
- [17] Gangnaik A S, Georgiev Y M and Holmes J D 2017 New generation electron beam resists: a review *Chem. Mater.* **29** 1898–917
- [18] Tatian B 1984 Fitting refractive-index data with the Sellmeier dispersion formula *Appl. Opt.* **23** 4477–85
- [19] D'Agostino R and Flamm D L 1981 Plasma etching of Si and SiO₂ in SF₆-O₂ mixtures *J. Appl. Phys.* **52** 162–7
- [20] Vitale S A, Chae H and Sawin H H 2001 Silicon etching yields in F₂, Cl₂, Br₂, and HBr high density plasmas *J. Vac. Sci. Technol. A* **19** 2197–206
- [21] Sivaramakrishnan S, Wang A, Gill P and Molnar A 2016 Design and characterization of enhanced angle sensitive pixels *IEEE Trans. Electron Devices* **63** 113–9

- [22] Marchetti R *et al* 2017 High-efficiency grating-couplers: demonstration of a new design strategy *Sci. Rep.* **7** 16670–7
- [23] David A *et al* 2006 Photonic-crystal GaN light-emitting diodes with tailored guided modes distribution *Appl. Phys. Lett.* **88** 061124
- [24] Keller S, Blagoi G, Lillemose M, Haefliger D and Boisen A 2008 Processing of thin SU-8 films *J. Micromech. Microeng.* **18** 1–10
- [25] Yasui M *et al* 2014 Effects of post exposure bake temperature and exposure time on SU-8 nanopattern obtained by electron beam lithography *Japan. J. Appl. Phys.* **53** 11RF03
- [26] Yang X *et al* 2007 Challenges in 1 Teradot. 2 dot patterning using electron beam lithography for bit-patterned media *J. Vac. Sci. Technol. B* **25** 2202–9
- [27] Schmid G M, Carpenter L E and Liddle J A 2004 Nonaqueous development of silsesquioxane electron beam resist *J. Vac. Sci. Technol. B* **22** 3497–502
- [28] Miller S A *et al* 2017 Low-loss silicon platform for broadband mid-infrared photonics *Optica* **7** 707–12
- [29] Zhang X *et al* 2019 Active matrix monolithic LED micro-display using GaN-on-Si epilayers *IEEE Photonics Technol. Lett.* **31** 865–8
- [30] Liu X-Q, Yu L, Ma Z-C and Chen Q-D 2017 Silicon three-dimensional structures fabricated by femtosecond laser modification with dry etching *Appl. Opt.* **56** 2157–61
- [31] Miller S A *et al* 2018 512-Element actively steered silicon phased array for low-power LIDAR 2018 *Conf. on Lasers and Electro-Optics, CLEO 2018—Proc.* (https://doi.org/10.1364/CLEO_AT.2018.JTh5C.2)
- [32] Belen R J, Gomez S, Kiehlbauch M and Aydil E S 2006 Feature scale model of Si etching in SF₆/O₂/HBr plasma and comparison with experiments *J. Vac. Sci. Technol. A* **24** 350–61
- [33] Goodyear A, Boettcher M, Stolberg I and Cooke M 2015 Direct comparison of the performance of commonly used e-beam resists during nano-scale plasma etching of Si, SiO₂, and Cr *Advanced Etch Technology for Nanopatterning IV* (<https://doi.org/10.1117/12.2085469>)
- [34] Nho Y C, Kang P H and Park J S 2004 The characteristics of epoxy resin cured by γ -ray and E-beam *Radiat. Phys. Chem.* **71** 243–6
- [35] Abadie M J M, Chia N K and Boey F 2002 Cure kinetics for the ultraviolet cationic polymerization of cycloliphatic and diglycidyl ether of bisphenol-A (DGEBA) epoxy systems with sulfonium salt using an auto catalytic model *J. Appl. Polym. Sci.* **86** 1587–91
- [36] Crivello J V and Lam J H W 1980 Complex triarylsulfonium salt photoinitiators: I. The identification, characterization, and syntheses of a new class of triarylsulfonium salt photoinitiators *J. Polym. Sci.* **18** 2677–95
- [37] Crivello J V and Lam J H W 1980 Complex triarylsulfonium salt photoinitiators: II. The preparation of several new complex triarylsulfonium salts and the influence of their structure in photoinitiated cationic polymerization *J. Polym. Sci.* **18** 2697–714
- [38] Barker I A and Dove A P 2013 Triarylsulfonium hexafluorophosphate salts as photoactivated acidic catalysts for ring-opening polymerisation *Chem. Commun.* **49** 1205–7
- [39] Martin C, Rius G, Llobera A, Voigt A, Gruetzner G and Pérez-Murano F 2007 Electron beam lithography at 10 keV using an epoxy based high resolution negative resist *Microelectron. Eng.* **84** 1096–9
- [40] Lin V J C and Koenig J L 1976 Raman studies of bovine serum albumin *Biopolymers* **15** 203–18
- [41] Dargaville B L *et al* 2011 Cross-linked poly(trimethylene carbonate-co-L-lactide) as a biodegradable, elastomeric scaffold for vascular engineering applications *Biomacromolecules* **12** 3856–69
- [42] Janz G J, Ambrose J, Coutts J W and Downey J R 1979 Raman spectrum of propylene carbonate *Spectrochim. Acta A* **35** 175–9
- [43] Peticolas W L 1995 Raman spectroscopy of DNA and proteins *Methods Enzymol.* **246** 389–416
- [44] Rygula A, Majzner K, Marzec K M, Kaczor A, Pilarczyk M and Baranska M 2013 Raman spectroscopy of proteins: a review *J. Raman Spectrosc.* **44** 1061–76
- [45] Williamson F and Shields E A 2003 SU-8 as an electron beam lithography resist *Biennial University/Government/Industry Microelectronics Symp.—Proc.* (<https://doi.org/10.1109/UGIM.2003.1225696>)
- [46] Pepin A 2004 Exploring the high sensitivity of SU-8 resist for high resolution electron beam patterning *Microelectron. Eng.* **73–74** 233–7
- [47] Aktary M, Jensen M O, Westra K L, Brett M J and Freeman M R 2003 High-resolution pattern generation using the epoxy novolak SU-8 2000 resist by electron beam lithography *J. Vac. Sci. Technol. B* **21** L5–L7
- [48] Chang T H P 1975 Proximity effect in electron-beam lithography *J. Vac. Sci. Technol.* **12** 1271–5
- [49] Yamazaki K, Kurihara K, Yamaguchi T, Namatsu H and Nagase M 1997 Novel proximity effect including pattern-dependent resist development in electron beam nanolithography *Japan. J. Appl. Phys.* **36** 7552–6
- [50] Van De Kraats A 2007 Proximity effect in e-beam lithography (<http://nanolithography.gatech.edu/proximity.pdf>)
- [51] Canalejas-Tejero V *et al* 2013 Ultrasensitive non-chemically amplified low-contrast negative electron beam lithography resist with dual-tone behaviour *J. Mater. Chem. C* **1** 1392–8
- [52] Della Giustina G, Prasciolu M, Brusatin G, Guglielmi M and Romanato F 2009 Electron beam lithography of hybrid sol-gel negative resist *Microelectron. Eng.* **86** 745–8
- [53] M technology GmbH 2000 ma-N 2400 and Mr-EBL 6000 - Negative Tone Photoresists (<https://www.microresist.de/en/produkt/mr-eb1-6000-series/>)